Valence Band Control of Metal Silicide Films via Stoichiometry Control

Frank Streller[†], Yubo Qi[‡], Jing Yang[‡], Filippo Mangolini[†§], Andrew M. Rappe[†‡], and Robert W. Carpick[†¶],*

[†] Department of Materials Science and Engineering, University of Pennsylvania, Philadelphia, PA 19104, United States. [‡] Makineni Theoretical Laboratories, Department of Chemistry, University of Pennsylvania, Philadelphia, PA 19104, United States. [¶] Department of Mechanical Engineering and Applied Mechanics, University of Pennsylvania, Philadelphia, PA 19104, United States.
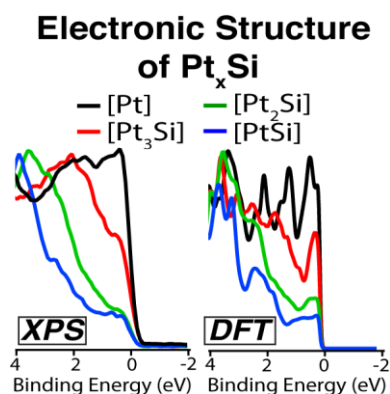
Corresponding Author

* carpick@seas.upenn.edu, phone number: 205-898-4608 (R.W.C.)

Present Addresses

§ Institute of Functional Surfaces, School of Mechanical Engineering, University of Leeds, LS2 9JT Leeds, United Kingdom.

The unique electronic and mechanical properties of metal silicide films renders them of interest as advanced materials in plasmonic devices, lithium-ion batteries, field-emitters, thermoelectric devices, field effect transistors, and nanoelectromechanical switches. However, enabling their use in such applications requires precisely controlling their electronic structure. Here, we use platinum silicide (Pt_xSi) as a metal silicide model system and demonstrate that the electronic state of Pt_xSi thin films ($1 \leq x \leq 3$) can be tuned between metallic and semimetallic by changing the silicide stoichiometry. Upon increasing the silicon content in Pt_xSi, the carrier density systematically decreases, as indicated by both valence band X-ray photoelectron spectroscopy and theoretical density of states (DOS) calculations. Among all Pt_xSi phases, Pt_3Si offers the highest DOS (approximately a threefold increase over PtSi), rendering it a promising material for a variety of novel applications. These results, demonstrating that the electronic structure of thin metal silicide films can be precisely tuned, suggest that metal silicides can be rationally designed to achieve the electronic properties required for specific applications.

TOC GRAPHIC.

Electronic Structure of Pt_xSi

— [Pt]   — [Pt_2Si]
— [Pt_3Si] — [PtSi]

XPS   DFT

Binding Energy (eV)   Binding Energy (eV)

KEYWORDS Platinum Silicide, Thin Film, X-ray Photoelectron Spectroscopy, Density of States, Resistivity, Density Functional Theory

Metal silicide (Me_xSi) thin films were extensively studied in the 1980s and have found use in the microelectronics industry as materials for electronic contacts, local interconnects, and diffusion barriers.[1] Recently, Me_xSi regained scientific attention as they are considered candidate materials for a variety of novel applications, such as plasmonics,[2] lithium-ion batteries,[3] field emitters,[4-6] thermoelectrics,[7-10] field-effect transistors,[11] and nanoelectromechanical switches.[12-14] The increasing popularity of Me_xSi is a consequence of their metal-like electrical properties, semiconductor-like thermal transport, mechanical robustness, and thermal stability. However, Boltasseva *et al.*[2] and Cheng *et al.*,[3] among others, pointed out that the composition and properties of Me_xSi need to be carefully optimized to fully utilize their potential in next-generation applications. We recently presented a methodology to precisely tune the composition of Me_xSi thin films by means of controlled solid-state diffusion.[15] This allows for the formation of platinum silicide (Pt_xSi) thin films over a wide composition range ($1 \leq x \leq 3$), including the novel Pt_3Si stoichiometry, with a significant range of mechanical and electronic properties.[12,14,15] While it is known that the Me_xSi composition strongly affects the resulting electrical, mechanical, and adhesive properties,[12,14] systematic studies determining the effect of Me_xSi composition on specific properties are lacking. Here, we compare valence band (VB) X-ray photoelectron spectroscopy (XPS) measurements with density of states (DOS) calculations to elucidate the relationship between composition and electronic structure/properties for Pt_xSi thin films.

Using source-limited solid-state diffusion (*i.e.,* films are formed by annealing of sequentially-deposited Pt and Si thin films of specific thickness ratios),[15] we fabricated Pt_xSi thin films of Pt_3Si, Pt_2Si, and PtSi. These films were interrogated using high-resolution VB XPS measurements to determine the DOS at the Fermi edge, which accurately determines the

electronic structure and many of the electronic properties of these Pt$_x$Si films. A high DOS at the Fermi edge is a requirement for having high electrical conductivity.[11] The Fermi edge shape therefore provides an indication of the electronic character of the tested material (metal, semimetal, or semiconductor) as shown schematically in Figure 1a. Metals are characterized by a large quantity of charge carriers (high density of states) near the Fermi edge that allows them to be efficient electrical conductors. Semimetals possess a significantly reduced DOS at the Fermi edge without an energy band gap (which, combined with their typically higher Seebeck coefficient and lower thermal conductivities compared to metals, makes them suitable thermoelectric materials).[16] The Fermi edges of semiconductors are located inside the band gap without any electronic states at the edge. Since XPS probes the occupied states of a material (see Figure 1b), the intensity of a valence band XPS spectrum directly correlates to the DOS. This relationship allows us to directly compare XPS measurements with theoretical DOS calculations.

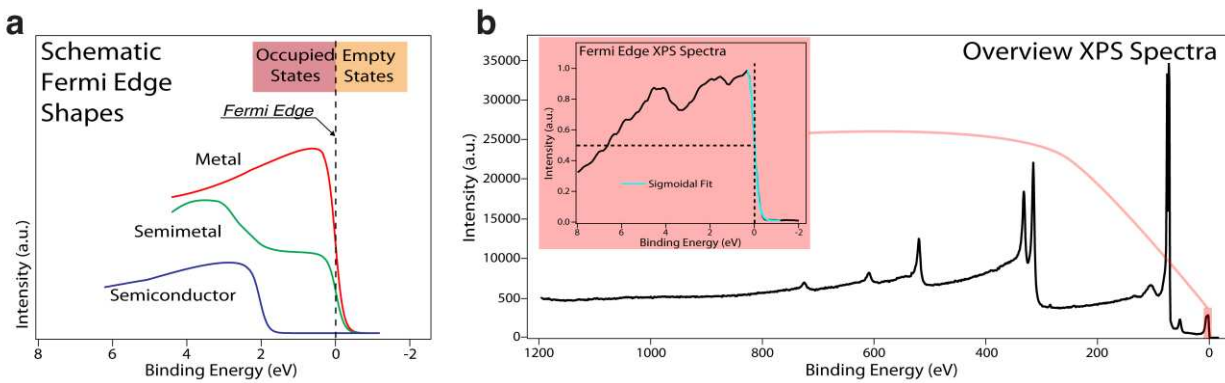**Figure 1:** Fermi edge shapes and locations in XPS spectra. **a.** Schematic Fermi edge shape of a metal, a semimetal, and a semiconductor. The intensity of charge carriers at the Fermi edge reduces from metals to semimetals and becomes zero for semiconductors. **b.** Location of the Fermi edge within an experimental Pt XPS spectrum. The Fermi edge is located at a binding energy value of 0 eV.

Figure 2 shows the results of the VB XPS measurements and the theoretical DOS calculations for [Pt], [Pt$_3$Si], [Pt$_2$Si], and [PtSi] films (the "[…]" notation refers to the achieved phase selectivity shown in Figure 2c). The composition of the produced Pt$_x$Si films was determined using quantitative XPS (see *Experimental and Computational Methods*). This demonstrated the phase selectivity as shown in Figure 2c; the [Pt$_3$Si] film was 74% Pt$_3$Si, the [Pt$_2$Si] film was 70% Pt$_2$Si, the [PtSi] film 92% PtSi, and the [Pt] film was 100% Pt. These exact compositions were also employed in the theoretical DOS calculations using a linear combination approach to ensure a better comparability of the results. The VB XPS measurements show a direct correlation between the Si concentration and the Fermi edge shape (Figure 2a). The experimental DOS at the Fermi edge systematically decreases with increasing Si concentration from Pt towards PtSi. The analyzed films show metallic and reduced-metallic Fermi edge shapes in the case of Pt and Pt$_3$Si, respectively, and typical semimetallic behavior for the Pt$_2$Si and PtSi films. The theoretical DOS calculations show a similar reduction of the DOS at the Fermi edge from Pt to PtSi. Additionally, the calculated DOSs for Pt, Pt$_2$Si, and PtSi are similar to those reported in previous works by Bentmann *et al.*[17] and Franco *et al.*[18] No DOS calculations for Pt$_3$Si have been previously reported in the literature.
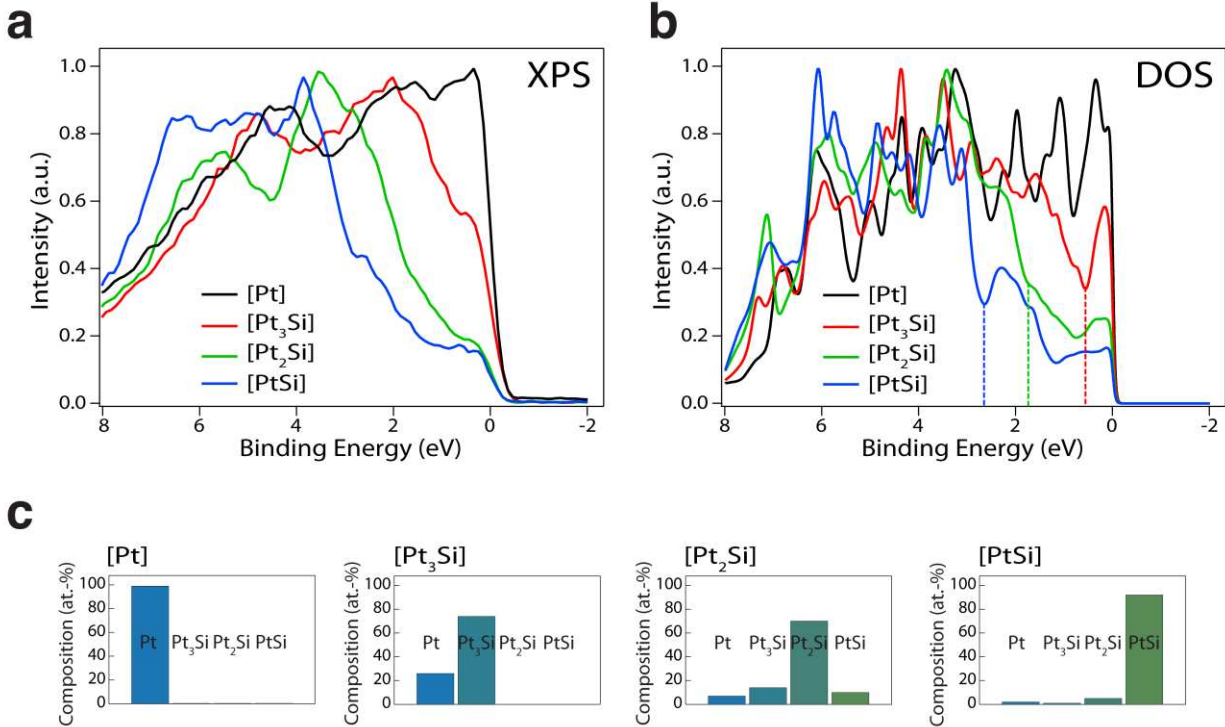
Figure 2: Experimental and theoretical Fermi edge shapes and compositions for [Pt], [Pt$_3$Si], [Pt$_2$Si], and [PtSi] samples. **a.** Experimental Fermi edge shapes of [Pt], [Pt$_3$Si], [Pt$_2$Si], and [PtSi] samples. Valence band electron population decreases with increasing Si-content of the silicide. **b.** Theoretical Fermi edge shapes of [Pt], [Pt$_3$Si], [Pt$_2$Si], and [PtSi] samples. Valence band electron population decreases with increasing Si-content of the silicide. The dotted vertical lines represent the location of the Pt$_{5d}$ manifold for PtSi (2.7 eV below Fermi edge), Pt$_2$Si (1.8 eV below Fermi edge), and Pt$_3$Si (0.5 eV below Fermi edge). **c.** Thin film composition of [Pt], [Pt$_3$Si], [Pt$_2$Si], and [PtSi] samples as determined from quantitative XPS measurements.

Figure 3 shows a direct comparison of the experimental and theoretical DOS for [Pt], [Pt$_3$Si], [Pt$_2$Si], and [PtSi] films. Overall, we find that all experimental Pt$_x$Si valence band spectra capture not only the general shape but also several individual features of the theoretical Pt$_x$Si DOS very well (Figure 3b-d). However, Figure 3a shows that the experimental Pt valence band

spectra is unable to resemble the structural detail of the theoretical Pt DOS. Comparison of our XPS with other XPS data show excellent agreement; comparison of our theoretical DOS and other DOS calculations show excellent agreement; but there is some disagreement between the two for the case of Pt.[19,20,21] This points towards an inherent difficulty in matching the valence band XPS spectrum of Pt to its theoretical DOS counterpart. The reasons for this phenomenon are discussed by Goldmann et al.[19] The intensity and shape of XPS valence band spectra of open d shell metals, such as Pt, are modified and therefore unable to resemble DOS calculations, due to: 1) instrumental resolution of the XPS system, 2) matrix element modulation across the width of the d-band, 3) lifetime of the photohole, 4) interaction of the photohole with the conduction electrons, and 5) inelastic electron scattering. The factor that most prominently influences the structural detail of the valence band spectra is the lifetime of the photohole, which leads to a broadening of the XPS peaks. These effects are less pronounced in Pt_xSi due to the filling up of the d shell due to silicidation, in agreement with our results.

The measured and calculated valence bands for Pt and the Pt_xSi films are dominated by the Pt_{5d} manifold. The Pt_{5d} position within the valence band greatly influences the observed Fermi edge shapes and consequently the carrier densities. A maximum of the Pt_{5d} manifold is located directly at the Fermi edge in the case of Pt (Figure 3a), whereas it shifts further away from the Fermi edge for Pt_xSi with increasing Si content. Our calculations show that the Pt_{5d} manifold of PtSi is shifted to approximately 2.7 eV below the Fermi edge, whereas the Pt_{5d} manifold of Pt_2Si is only shifted to approximately 1.8 eV below the Fermi edge (see dotted vertical lines in Figure 2b), similar to previously reported values.[17,18] The novel Pt_3Si films show a shift of the Pt_{5d} manifold of only approximately 0.5 eV, which results in a metallic-like character of the Fermi edge.
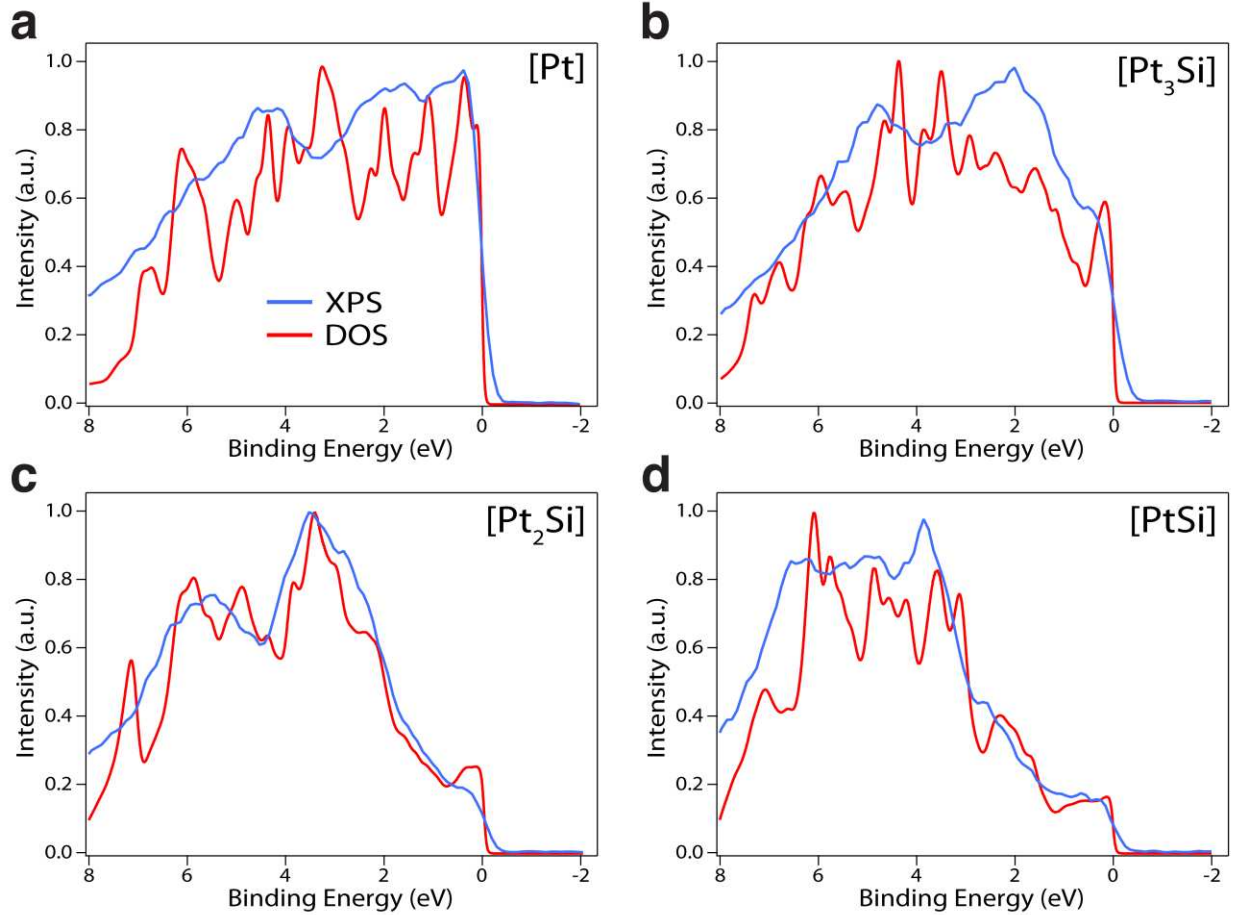
Figure 3. Comparison between experimental and theoretical Fermi edge shapes for [Pt], [Pt$_3$Si], [Pt$_2$Si], and [PtSi] samples. **a.** [Pt] sample (100% metallic Pt). **b.** [Pt$_3$Si] sample (which includes 74 % Pt$_3$Si). **c.** [Pt$_2$Si] sample (which includes 70% Pt$_2$Si). **d.** [PtSi] sample (which includes 92% PtSi).

Table 1 quantitatively compares the experimental and calculated DOS of Pt, Pt$_3$Si, Pt$_2$Si, and PtSi by means of their normalized carrier densities. The carrier densities were obtained by integrating the experimental and theoretical DOS within a $2k_BT$ (~ 0.05eV for T = 300K) energy window around the Fermi edge.[11] The normalized carrier densities computed from the VB XPS measurements are in excellent agreement with the DOS calculations and confirm the systematic decrease in carrier density with increasing Si-content. The PtSi and Pt$_2$Si films were found to

possess approximately 17-19% and 20-28% of the carrier density of Pt, respectively. These values are in good agreement with theoretical calculations performed by Bentmann *et al.*[17] The Pt-rich Pt_3Si film possesses a very high carrier density of 59-61% of the DOS of Pt, which is a more than 3-fold improvement over the PtSi carrier density.

Table 1. Normalized carrier densities computed from VB XPS experiments and DOS calculations and measured sheet resistance values.

	Normalized Carrier Density		**Sheet Resistance ($\Omega/\square$)**
	VB XPS	*DOS Calculation*	
Pt	1	1	2.6
Pt_3Si	0.59	0.61	18.9
Pt_2Si	0.20	0.28	31.8
PtSi	0.17	0.19	57.6

As mentioned above, a high DOS at the Fermi level is one of the requirements for having a high electrical conductivity. We performed four point probe measurements on the Pt, Pt_3Si, Pt_2Si, and PtSi films to determine the sheet resistance as an inverse measure of the electrical conductivity (Figure 4). The measured sheet resistance values show a systematic decrease in electrical conductivity from Pt to PtSi, which confirms the expected qualitative trend of the carrier density. The sheet resistance values for Pt, Pt_3Si, Pt_2Si, and PtSi were measured as 2.6, 18.9, 31.8, and 57.6 $\Omega/\square$, respectively. The corresponding resistivity values were calculated as 10.6, 75.5, 127.2, and 230.4 $\mu\Omega$-cm, respectively. The obtained sheet resistance and resistivity values for Pt, Pt_2Si and PtSi are in good agreement with results reported in other works.[22,23]
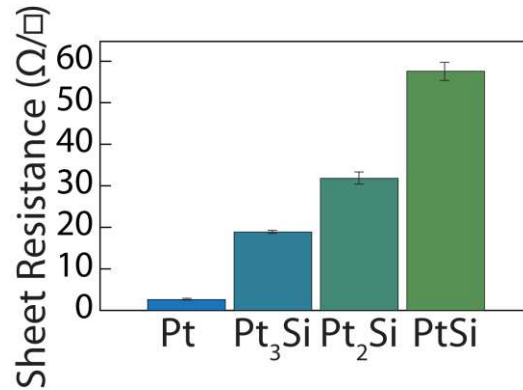
Figure 4. Sheet resistance of [Pt], [Pt$_3$Si], [Pt$_2$Si], and [PtSi] samples.

The high electrical conductivity (and correspondingly, the low sheet resistance and resistivity) of Pt$_3$Si compared to Pt$_2$Si and PtSi could motivate the use of Pt$_3$Si in several applications as a replacement for Pt$_2$Si or PtSi. Most notably for the semiconductor industry, where PtSi is considered as an attractive contact material to the source, drain, and gate for CMOS field effect transistors because of its low Schottky barrier and high thermal stability. However, PtSi suffers from low electrical conductivity due to its low DOS, which this work has verified. Recent work by Slepko and Demkov investigates Ti-doping of PtSi in an attempt to increase its DOS and thereby its electrical conductivity.[11] The researchers succeeded in increasing the DOS of PtSi by approximately 1.7 times through doping with 12.5 at.% Ti. However, while the Ti doping increased the DOS it also introduced Ti impurities that act as scattering centers and decrease the electrical conductivity. Here we were able to show that the Pt$_3$Si phase could solve these issues by inherently possessing a high DOS (approximately 3.4 times higher than DOS of PtSi) and a low sheet resistance and resistivity indicating a high electrical conductivity. Since no doping is necessary to achieve this high DOS, Pt$_3$Si does not suffer from additional creation of scattering centers.

In summary, we show that the electronic structure and properties of Pt_xSi thin films can be tuned for specific applications between metallic and semimetallic properties by controlling the film stoichiometry. The comparison of valence band X-ray photoelectron spectroscopy spectra with theoretical density functional theory calculations shows that the density of states of Pt_3Si is significantly higher than that of Pt_2Si and $PtSi$. The resulting high electrical conductivity of Pt_3Si makes this stoichiometry particularly interesting for applications that demand high electrical conductivity combined with high thermal and mechanical stability.[12] This work on Pt_xSi provides a framework for studying the tunability of the electrical properties of other metal silicides based on Ni, Cu, Au, Fe, Co, Pd, Ag, and Rh among others. We expect that the open d shell metals (e.g. Fe, Co, Pd) exhibit the strongest tunability of the electrical properties due to their similarity with Pt, which was shown to have a strong compositional dependence of the Pt_{5d} manifold position.

EXPERIMENTAL AND COMPUTATIONAL METHODS

Thin film formation. To form the Pt_xSi films, Pt and *a*-Si films were sputter-deposited in a Denton Vacuum Explorer 14 sputterer (Denton Vacuum Inc., Moorestown, NJ) with a purity of 99.99% for both films and subsequently annealed under high vacuum (10^{-7} Torr) at 600 °C for 10 min (heating rate 30 °C/min). Pt was deposited in dc mode at 450 W and *a*-Si in ac mode at 230 W. The thicknesses of the Pt and *a*-Si films were chosen to obtain nearly pure phases of Pt_3Si, Pt_2Si, and $PtSi$ upon annealing.[15] The Pt and *a*-Si depositions were conducted sequentially in the same deposition system under maintained vacuum. This minimizes contaminant adsorption between the layers and oxidation of the a-Si, both of which are inhibiting factors for silicidation.

X-ray photoelectron spectroscopy analysis. The chemistry of the near-surface region was investigated by XPS using a customized XPS spectrometer (VG Scienta AB, Uppsala, Sweden).[24] XPS analyses were performed using a monochromatic Al Kα source (photon energy 1486.6 eV). The residual pressure in the analysis chamber was consistently less than 1×10^{-8} Torr. The spectrometer was calibrated according to ISO 15472:2001 with an accuracy of ±0.05 eV. Survey and high-resolution spectra were acquired in constant-analyzer-energy mode with the pass energies of 200 and 100 eV, respectively. The full width at half-maximum (FWHM) of the peak height for the high resolution Ag 3d5/2 signal of a sputter-cleaned Ag sample was 0.57 eV. The spectra were processed using CasaXPS software (v.2.3.16, Casa Software Ltd., Wilmslow, Cheshire, U.K.). Background subtraction was performed using the Shirley−Sherwood method. The quantitative evaluation of XPS data, as described in ref **25**, was based on integrated intensity using a first-principles model and applying Powell's equation. The inelastic mean free path was calculated using the TPP-2M formula.[26] Curve synthesis for the Pt 4f peaks was performed by constraining the integrated intensity ratio of these two signals to 3:4 and their energy separation to 3.33 eV. The reference energies for Pt $4f_{7/2}$ peaks are 71.05, 71.55, 72.18, and 72.75 eV for Pt, Pt_3Si, Pt_2Si, and PtSi, respectively, and are in agreement with literature values.[12,15] The Pt 4f peaks have been chosen to determine sample surface chemistry due to their high intensity and the high sensitivity of their position to the Pt_xSi stoichiometry, in contrast with the less intense and less stoichiometrically-sensitive position of the Si 2p peaks.

Theoretical density of states calculations. Density functional theory (DFT) calculations were performed on PtSi, Pt_2Si, Pt_3Si and Pt with generalized gradient approximation[27] (GGA) exchange-correlation functionals implemented in QUANTUM ESPRESSO package.[28] We used norm-conserving plane-wave pseudopotentials for all the species.[29-31] The kinetic energy cutoff

12

to the wavefunction expansion is E_{cut}= 680 eV. An 8×8×8 Monkhorst-Pack[32] grid k–point mesh

was used to sample Brillouin-zone (BZ) in structural optimization, while a denser one 24×24×24

was used for density of states (DOS) calculation. The occupation of the states around the Fermi

energy E_F was calculated from the Fermi-Dirac distribution[33]

$$f(E) = \frac{1}{e^{(E-E_F)/kT} + 1}$$

where $f(E)$ is the occupation probability for the state with energy E, k is the Boltzmann constant

and T is the temperature, which was selected as 298 K. The DOS for a non-pure compound was

estimated from a linear combination of the DOS of its each component.

AUTHOR INFORMATION

Corresponding Author

* carpick@seas.upenn.edu (R.W.C.)

Present Addresses

§ Institute of Functional Surfaces, School of Mechanical Engineering, University of Leeds, LS2

9JT Leeds, United Kingdom.

Author Contributions

F.S. prepared the samples and carried out the XPS experiments and resistivity measurements.

Y.Q. and J.Y. performed the DOS calculations. A.M.R. oversaw the DOS calculation. F.M

oversaw the XPS measurements. R.W.C. supervised the research. F.S. wrote the manuscript.

Y.Q., J.Y., F.M., A.M.R. and R.W.C. edited the manuscript.

Notes

REFERENCES

(1) Miglio, L.; d'Heurle, F. *Silicides - Fundamentals and Applications*; World Scientific Publishing: Singapore, 2000.

(2) Naik, G. V.; Shalaev, V. M.; Boltasseva, A. Alternative plasmonic materials: Beyond gold and silver. *Adv. Mater.* **2013**, 25, 3264−3294.

(3) Liu, C.; Li, F.; Ma, L.-P.; Cheng, H.-M. Advanced materials for energy storage. *Adv. Mater.* **2010**, 22, E28−E62.

(4) Lin, H.-K.; Cheng, H.-A; Lee, C.-Y.; Chiu, H.-T. Chemical vapor deposition of TiSi nanowires on C54 TiS2 thin film: An amorphous titanium silicide interlayer assisted nanowire growth. *Chem. Mater.* **2009**, 21, 5388−5396.

(5) Li, H.; Wu, J.; Wang, Z. M. *Silicon-Based Nanomaterials*; Springer: Berlin, 2013.

(6) Higgins, J. M.; Ding, R.; Jin, S. X. Synthesis and characterization of manganese-rich silicide (α-Mn5Si3, β-Mn5Si3, and β-Mn3Si) nanowires. *Chem. Mater.* **2011**, 23, 3848−3853.

(7) Rowe, D. M. *Thermoelectrics Handbook: Macro to Nano*; Taylor & Francis Group: Abingdon, 2006.

(8) Fedorov, M. I. Thermoelectric Silicides: Past, Present and Future. *J. Thermoelectr.* **2009**, 2, 51−60.

(9) Itoh, T.; Yamada, M. Synthesis of thermoelectric manganese silicide by mechanical alloying and pulse discharge sintering. *J. Electron. Mater.* **2009**, 38, 925−929.

(10) de Boor, J.; Dasgupta, T.; Kolb, H.; Compere, C.; Kelm, K.; Mueller, E. Micostructural effects on thermoelectric efficiency: A case study on magnesium silicide. *Acta Mater.* **2014**, 77, 68−75.

(11) Slepko, A.; Demkov, A. A. Band engineering in silicide alloys. *Phys. Rev. B.* **2012**, 85, 035311.

(12) Streller, F.; Wabiszewski, G. W.; Mangolini, F.; Feng, G.; Carpick, R. W. Tunable, source-controlled formation of platinum silicides and nanogaps from thin precursor films. *Adv. Mater. Interfaces* **2014**, 1, 1300120.

(13) Loh, O. Y.; Espinosa, H. D. Nanoelectromechanical contact switches. *Nat. Nanotechnol.* **2012**, 7, 283−295.

(14) Streller, F.; Wabiszewski, G. E.; Carpick, R. W. Next-generation nanoelectromechanical switch contact materials. *IEEE Nanotechnol. Mag.* **2015**, 9, 18−24.

(15) Streller, F.; Agarwal, R.; Mangolini, F.; Carpick, R. W. Novel metal silicide thin films by design via controlled solid-state diffusion. *Chem. Mater.* **2015**, 27, 4147−4253.

(16) Bubnova, O.; Khan, Z. U.; Wang, H.; Braun, S.; Evans, D. R.; Fabretto, F.; Hojati-Talemi, P.; Dagnelund, D.; Arlin, J.-P.; Geerts, Y. H.; Desbief, S.; Breiby, D. W.; Andreasen, J. W.; Lazzaroni, R.; Chen, W. M.; Zozoulenko, I.; Fahlman, M.; Murphy, P. J.; Berggren, M.; Crispin, X. Semi-metallic polymers. *Nat. Mater.* **2014**, 13, 190−194.

(17) Bentmann, H.; Demkov, A. A.; Gregory, R.; Zollner, S. Electronic, optical, and surface properties of PtSi thin films. *Phys. Rev. B.* **2008**, 78, 205302.

(18) Franco, N.; Klepeis, J. E.; Bostedt, C.; Van Buuren, T.; Heske, C.; Pankratov, O.; Terminello, L. J. Valence band study of PtSi by synchrotron radiation photoelectron spectroscopy. *J. Electron. Spectrosc.* **2001**, 114−116, 1191−1196.

(19) Hoechst, H.; Huefner, S.; Goldmann, A. XPS-valence bands of iron, cobalt, palladium and platinum. *Phys. Lett.* **1976**, 57A, 265−266.

(20) Strasser, P.; Koh, S.; Anniyev, T.; Greeley, J.; More, K.; Yu, C.; Liu, Z.; Kaya, S.; Nordlund, D.; Ogasawara, H.; Toney, M. F.; Nilsson, A. Lattice-strain control of the activity in dealloyed core-shell fuel cell catalysts. *Nature Chem.* **2010**, 2, 454−460.

(21) Krupski, K.; Moors, M.; Jozwik, P.; Kobiela, T.; Krupski, A. Structure determination of Au on Pt(111) surface: LEED, STM and DFT study. *Materials* **2015**, 8, 2935−2952.

(22) Powell, R. W.; Tye, R. P.; Woodman, M. J. Thermal conductivities and electrical resistivities of the platinum metals. *Platinum Metals Rev.* **1962**, 6, 138-143.

(23) Conforto, E. *Formation and properties of nanometer-thick platinum silicide layers*. PhD. Thesis, Ecole Polytechnique Federale Du Lausanne, 1996.

(24) Mangolini, F.; Ahlund, J.; Wabiszewski, G. E.; Adiga, V. P.; Egberts, P.; Streller, F.; Backlund, K.; Karlsson, P. G.; Wannberg, B.; Carpick, R. W. Angle-resolved environmental X-ray photoelectron spectroscopy: A new laboratory setup for photoemission studies at pressures up to 0.4 Torr. *Rev. Sci. Instrum.* **2012**, 83, 093112.

(25) Mangolini, F.; Rossi, A.; Spencer, N. D. Chemical reactivity of triphenyl phosphorothionate (TPPT) with iron: An ATR/FT-IR and XPS investigation. *J. Phys. Chem. C* **2011**, 115, 1339−1354.

(26) Tanuma, S. *Surface Analysis by Auger and X-ray Photoelectron Spectroscopy*; IM Publications: Charlton, U.K., 2003.

(27) Perdew, J. P.; Burke, K.; and Ernzerhof M. Generalized Gradient Approximation Made Simple. *Phys. Rev. Letts.* **1996**, 77, 3865−3868

(28) Giannozzi, P.; Baroni, S.; Bonini, N.; Calandra, M.; Car, R.; Cavazzoni, C.; Ceresoli, D.; Chiarotti, G. L.; Cococcioni, M.; Dabo, I.; Corso, A. D.; de Gironcoli, S.; Fabris, S.; Fratesi, G.; Gebauer, R.; Gerstmann, U.; Gougoussis, C.; Kokalj, A.; Lazzeri, M.; Martin–Samos, L.; Marzari, N.; Mauri, F.; Mazzarello, R.; Paolini, S.; Pasquarello, A.; Paulatto, L.; Sbraccia, C.; Scandolo, S.; Sclauzero, G.; Seitsonen, A. P.; Smogunov, A.; Umari, P.; Wentzcovitch, R. M. Quantum ESPRESSO: A Modular and Open–Source Software Project for Quantum Simulations of Materials. *J. Phys.: Condens. Matter* **2009**, 21, 395502–395520.

(29) Ramer, N. J.; Rappe, A. M. Designed nonlocal pseudopotentials for enhanced transferability. Phys. Rev. B **1999**, 59, 12471−12478.

(30) Rappe, A. M.; Rabe, K. M.; Kaxiras, E.; Joannopoulos, J. D. Optimized pseudopotentials. *Phys. Rev. B* **1990**, 41(2), 1227.

(31) http://opium.sourceforge.net.

(32) Monkhorst, H. J.; Pack, J. D. Special Points for Brillouin–Zone Integrations. *Phys. Rev. B* **1976**, 13, 5188–5192.

(33) Kittel, C. *Introduction to Solid State Physics*; John Wiley & Sons, Inc.: Toronto, Canada, 1971.